Research Article

Hydro-Mechanical Constraints and Deformations in Road Embankments Using Unsaturated Low-Swelling Soil

¹Soumaïla Gandema, ¹Marcel Bawindsom Kébré, ^{1,2}Rimyalegdo Kiébré, ¹François Dabilgou, ¹Timbe N'Djédanoum and ¹Guillaume Zamantakonè Ki

Article history Received: 18-02-2025 Revised: 16-04-2025 Accepted: 02-05-2025

Corresponding Author: Soumaïla Gandema Laboratoire de Matériaux et Environnement, Université Joseph KI-ZERBO, Ouagadougou, Burkina Faso Email: soumaila_gandema@ujkz.bf **Abstract:** In this paper, we present the results of a simulation of the evolution of stresses and deformations in a road embankment using unsaturated lowswelling soil under hydro-mechanical pressures, modeled with the finite element code Code Bright. We assume that this embankment, which supports asphalt, follows the Barcelona Thermo-Elasto-Plastic model (BBM-TEP). This model describes the Thermo-Hydro-Mechanical (THM) behavior of unsaturated fine soils based on variations in net stress and suction. Through this simulation, the analysis focuses on the collapse of road structures, which is generally due to the poor quality of materials used but also to natural phenomena such as capillary rise and anthropogenic factors such as overloading. It was found that capillary rise leads to an increase in the degree of saturation by more than 50% at the edges of the structure and deformations of up to one centimeter when additional loads are applied to the embankment surface. The behavior of unsaturated soils is also highlighted, such as the decrease in void ratio with increasing effective stress or suction and the increase in suction with effective stress.

Keywords: Low-Swelling Soil, Road Fill, Capillary Rise, Overloading, Collapses

Introduction

The structure of a road typically comprises the earthwork portion, which includes the embankment and subgrade, and the pavement, which consists of base and surface layers. The embankment and subgrade must be constructed to meet both short-term requirements (ensuring the mobility of construction vehicles, enabling the compaction of upper layers, meeting leveling requirements, and protecting the subgrade while awaiting pavement construction) and long-term requirements (homogenizing the bearing capacity of the underlying soil, protecting the pavement from fluctuations in the moisture content of the supporting soil, ensuring thermal protection of the supporting soil, and contributing to pavement drainage) (GTR, 2023). In fact, an embankment should maintain a stable geometry after construction. However, using poorquality materials compromises its internal stability, increasing the risk of failure. In such cases, plastic deformations are likely to occur due to differential settlements that are incompatible with the desired level of service (Morsy et al., 2023; Mridakh et al., 2022).

In Burkina Faso, as well as in the Sahelian regions in general, the most common soil types are sandy-silty soils (72.5% of the total area), followed by sandy-clayey soils (15.5%), silty soils (9.3%), and sandy-clayey soils (12%) (Alvar-Beltrán et al., 2021). These soils, often swelling or slightly swelling, are not suitable for use in the foundations of road construction projects. Roads are subjected to various mechanical (traffic load), thermal (sun exposure), and hydric (capillary rise, climatic events such as floods or droughts, and human activities nearby, such as excessive irrigation or water pipe leaks) stresses. These phenomena have become critical in developing countries today. Such stresses can significantly alter soil properties, threatening the stability and durability of infrastructure. (Morsy et al., 2023; Mridakh et al., 2022), especially when these materials are used for constructing platforms. In response to these challenges, large quantities of coarse soil, often lateritic, are commonly brought in from borrow areas, which are becoming increasingly scarce and distant from construction sites. In addition to the scarcity of this resource, transportation and extraction



¹Laboratoire de Matériaux et Environnement, Université Joseph KI-ZERBO, Ouagadougou, Burkina Faso ²Département de Physique, Université Lédea Bernard OUEDRAOGO, Ouahigouya, Burkina Faso

operations have negative environmental impacts (pollution due to machinery emissions, increased aerosols in the environment, etc.) as well as social repercussions, including the loss of potential agricultural land for local populations. To reduce the systematic use of coarse materials, the use of locally available materials close to construction sites is emerging as a viable alternative (Grossegger et al., 2024; Hudaykulov & Aralov, 2024; Hudaykulov, Rashidbek et al., 2024; Rahla et al., 2021; Tulebekova et al., 2024), especially in the context of the call to build a circular economy that protects the environment (Pereira & Vieira, 2022). However, the reuse of these local soils in road embankments is only feasible after appropriate treatment that enables them to achieve the required performance to withstand the mechanical and environmental stresses to which they will be subjected.

Previous studies have focused on the use of fine soils in embankments (Droniuc, 2013; Ghosh *et al.*, 2021; Pallav *et al.*, 2023; Sadeghabadi *et al.*, 2021; Showkat *et al.*, 2022). Many of these studies have simulated the hydro-mechanical and thermo-hydro-mechanical behavior of compacted fine soils in unsaturated conditions (Ali *et al.*, 2021; Droniuc, 2013; Kayadelen *et al.*, 2022; Prajapati, Vikas & Das, Arghya, 2023) and their stabilization through lime/cement treatment or hydraulic binders (Bakaiyang *et al.*, 2022; Chaiyaput *et al.*, 2022; Khemissa & Mahamedi, 2014; Kired *et al.*, 2023; Vukićević *et al.*, 2019).

In this paper, a numerical simulation of a road embankment with imposed boundary conditions was performed using the finite element calculation program CODE_BRIGHT, which employs the Barcelona thermoelasto-plastic model BBM-TEP (Olivella *et al.*, 2024). The pre- and post-processing graphical interface GiD was used to input the data for the calculation, the geometry of the structure, and the initial and boundary conditions. The results obtained allowed us to analyze the collapse of road structures due to natural phenomena such as capillary rise and anthropogenic factors such as overloading. Through the results of this simulation, the general behavior of unsaturated soils subjected to thermo-hydro-mechanical stresses was also analyzed.

Materials and Methods

Barcelona Thermo-Elasto-Plastic Model (BBM-TEP) for Unsaturated Low-Swelling Soils

The Barcelona Basic Model (BBM) - Thermoelastoplastic (TEP), a Thermo-Hydro-Mechanical Behavior of Expansive Clays model presented in the CODE_BRIGHT user's guide by Olivella *et al.* (2024), is used for modeling the behavior of the road embankment. The database on the numerical modeling of embankments on compressible soils

conducted by Mestat (2001) identifies this model as the most advanced and widely used to capture the fundamental characteristics of the behavior of low-swelling soils (sands, silts, sandy clays, and low-plasticity clays) in unsaturated conditions. It is based on the theory of elasto-plasticity and formulated for isotropic and triaxial stress states (Olivella *et al.*, 2024).

Formulation of Balance Equations

The following formulation is a deduced version from that presented by (Gens & Sánchez, 2014). Isothermal conditions are considered in constitutive equations, so phenomena such as vapour transport are neglected. Only the equilibrium balances of water, gas, solid and momentum are taken into account.

Mass Balance of Water

$$\frac{\partial}{\partial t} \left(\theta_l^w S_l \phi + \theta_g^w S_g \phi \right) + \nabla \cdot \left(j_l^w + j_g^w \right) = f^w \tag{1}$$

In this equation, θ_l^w and θ_g^w are volumetric water content of liquid and gas phase respectively; ϕ , the soil porosity and S_α ($\alpha = l, g$), The proportion of the pore volume that is occupied by the alpha phase. J^i and J_g are the overall mass fluxes of water in the liquid and gas phases, respectively. f^w represents the external mass influx of water per unit volume within the soil.

Mass Balance of Air

$$\frac{\partial}{\partial t} \left(\theta_l^a S_l \phi + \theta_g^a S_g \phi \right) + \nabla \cdot \left(j_l^a + j_g^a \right) = f^a \tag{2}$$

For air (denoted a in exponent) and in the liquid (indexed l) and gas (indexed g) phases, θ_l^a and θ_g^a are the mass concentration; j_l^a and j_g^a , the overall mass fluxes and f^a , the external mass influx.

Mass Balance of Solid

The variation in porosity, as a function of changes in solid density and the volumetric deformation of the solid framework, is derived from the following solid mass balance equation:

$$\frac{\partial}{\partial t} \left(\rho_t (1 - \phi) \right) + \nabla \cdot \left(\rho_t (1 - \phi) \dot{u} \right) = 0 \tag{3}$$

 \dot{u} denotes the velocity vector of the solid.

Momentum Balance for the Medium

$$\nabla \cdot \sigma_t + b = 0 \tag{4}$$

Where σ_t represents the total stress tensor and b the vector of body forces. Inertial terms have not been taken into count in this equation. Low velocities and accelerations of

the medium allow to neglect inertial terms in comparison with stress terms. A low strain rate is therefore assumed.

Constitutive Equations of BBM-TEP

The constitutive equations presented in this section are organized into two categories: hydrodynamic and mechanical aspects.

Hydrodynamic Considerations

Generalized Darcy's law as used for fluid phase advective flux into the medium:

$$q_{\alpha} = -K_{\alpha}(\nabla P_{\alpha} - \rho_{\alpha}g) \ \alpha = l, g \tag{5}$$

In this equation, P_{α} is the pressure of α phase in the medium. K_{α} is the permeability tensor of α phase in the medium, expressed as follows:

$$K_{\alpha} = k \frac{k_{r\alpha}}{\mu_{\alpha}} \alpha = l, g \tag{6}$$

k is the intrinsic permeability tensor; μ_{α} , the dynamic viscosity of the α phase; $k_{r\alpha}$, the α phase relative permeability written generally in terms of the phase degree of saturation S_e . In this study, for the liquid phase, we use the following relationship with A and λ as model fitting parameters:

$$k_{rl} = AS_e^{\lambda} \tag{7}$$

The popular van Genuchten model (1980) is used to describe the effective degree of saturation S_e (-) as a function of soil suction s:

$$S_e = \frac{S_l - S_{rl}}{S_{ls} - S_{rl}} = \left(1 + \left(\frac{s}{p}\right)^{\frac{1}{1-\lambda}}\right)^{-\lambda} \tag{8}$$

Where S_l (-) is the degree of saturation of the liquid phase; S_{rl} (-) is the residual liquid saturation; S_{ls} (-) is the maximum saturation; and P (MPa) and λ (-) are the model parameters.

The Kozeny model (1927) is adopted to describe the intrinsic permeability of the material. This model assumes that the intrinsic permeability tensor k of a porous material undergoing volumetric deformations is a function of its porosity (Olivella *et al.*, 2024):

$$k = k_0 \frac{\phi^3}{(1-\phi_0)^2} \frac{(1-\phi_0)^2}{\phi_0^3} \tag{9}$$

Where ϕ *is* the porosity, ϕ_0 is the reference porosity, and k_0 is the intrinsic permeability corresponding to ϕ_0 .

Mechanical Behaviors

The mechanical behavior of the material can be expressed in an incremental form to relate stress and strain variations (Olivella *et al.*, 2024):

$$d\underline{\sigma}' = D_e d\underline{\varepsilon} - \xi D_e \frac{\partial G^p}{\partial \sigma'} - D_e h_e \underline{I} ds \tag{10}$$

Where $d\sigma'$ which is described as the increment of the effective stress tensor; $d\varepsilon = d\varepsilon^e + d\varepsilon^p$ is the sum of the increments of elastic and plastic strains, $\xi(-) > 0$ is the plastic multiplier, $G^p(-)$ is the plastic potential, I is the identity tensor and ds represents the increment of suction. In this model, the elastic matrix D_e represents the stiffness matrix or constitutive matrix of the material within the framework of elastic deformations. This matrix describes the linear relationship between the applied stresses and the induced strains in the material under the assumption of reversible elastic behavior. Specifically, the matrix D_e is used to define the elastic behavior of unsaturated soil, incorporating the bulk modulus K (MPa) and the shear modulus G (MPa), which are functions of the hydric conditions and suction in the material. This matrix is essential for determining how the material responds to mechanical loading in the elastic phase before plastic deformations occur. D_e is given by:

$$D_{e} = \begin{pmatrix} K + \frac{4}{3}G & K - \frac{2}{3}G & K - \frac{2}{3}G & 0 & 0 & 0 \\ K - \frac{2}{3}G & K + \frac{4}{3}G & K - \frac{2}{3}G & 0 & 0 & 0 \\ K - \frac{2}{3}G & K - \frac{2}{3}G & K + \frac{4}{3}G & 0 & 0 & 0 \\ 0 & 0 & 0 & G & 0 & 0 \\ 0 & 0 & 0 & 0 & G & 0 \\ 0 & 0 & 0 & 0 & 0 & G \end{pmatrix}$$
(11)

The term h_e (-) is a vector that accounts for the effect of suction changes on elastic deformations and is defined by $h_e = D_e^{-1} F_e$, with F_e given by:

$$F_{e} = \begin{pmatrix} K\left(\frac{\kappa_{s}}{1+e}\right)\left(\frac{1}{s+p_{atm}}\right) \\ K\left(\frac{\kappa_{s}}{1+e}\right)\left(\frac{1}{s+p_{atm}}\right) \\ K\left(\frac{\kappa_{s}}{1+e}\right)\left(\frac{1}{s+p_{atm}}\right) \\ 0 \\ 0 \\ 0 \end{pmatrix}$$

$$(12)$$

Where κ_s (-) is the compressibility coefficient for suction increments in the elastic domain, $s = u_a - u_w$ is the suction, e(-) the void ratio and p_{atm} (MPa) the atmospheric pressure.

In this model, Olivella *et al.* (2024) introduced an elastoplastic constitutive framework characterized by a generalized yield surface that incorporates both stress and suction effects. For convenience, the isothermal saturated reference constitutive behavior has been represented using a variant of the classical Modified Cam-Clay model (Olivella *et al.*, 2024).

$$F^{LC}(p^*,q,s) = q^2 - M^2(p^* + p_s(s))(p_0(s) - p^*) = 0$$
(13)

 $q = \sigma_1 - \sigma_3$ is the deviatoric stress, $p' = \frac{1}{3}(\sigma_1' + \sigma_2' + \sigma_3') = p - max(u_a - u_w)$ is the mean net stress; M(-) is the critical state line slope, taken constant in this study. $p_0(s)$ and $p_s(s)$ are function of soil suction and define by:

$$p_0(s) = p_c \left(\frac{p_0^*}{p_c}\right)^{\frac{\lambda(0) - \kappa_{i0}}{\lambda(s) - \kappa_{i0}}} p_s(s) = ks$$
 (14)

Where $\lambda(s) = \lambda(0)[r + (1 - r) exp(-\beta s)]$ is the slope of the virgin compression curve at suction $s; p_0^*$ represents the saturated preconsolidation stress; p_c is a reference stress; k controls the increase in the tensile strength with suction; r and β control the rate of increase of soil stiffness with suction; κ_{i0} is the initial (s = 0) elastic slope for specific volume-mean stress relationship.

The elastic volumetric strain is given by:

$$d\varepsilon_{v}^{e} = \frac{\kappa_{io}}{1+e} \frac{dp'}{p'} + \frac{\kappa_{so}}{(1+e)} \frac{ds}{(s+p_{atm})}$$

$$\tag{15}$$

Where κ_{s0} is the initial (s=0) elastic slope for specific volume-suction relationship.

Hardening corresponds to the evolution of yield curve LC (Eq. 13) in the isotropic p' - s plane, and depends on plastic volumetric strain according to:

$$\frac{dp_0^*}{p_0^*} = \frac{1+e}{\lambda(0)-\kappa} d\varepsilon_v^p \tag{16}$$

Where κ denotes the elastic stiffness parameter associated with variations in the net mean stress.

The plastic potential in (Eq.17) is associated to the hardening rule and it is defined by:

$$G^{p} = \alpha q^{2} - M^{2} (p^{*} + p_{s}(s)) (p_{0}(s) - p^{*})$$
 (17)

Where:

$$\alpha = \frac{M(M-9)(M-3)}{9(6-M)} \left[\frac{1}{1 - \frac{K}{\lambda(0)}} \right]$$
 18)

Is a non-asociativity parameter.

Figure 1 illustrates the general configuration of the yield surface within the in p-q-s space, highlighting the key characteristics of the BBM, including The Loading-Collapse (LC) and Suction-Increase (SI) yield curves.

Material and Characteristics

In this article, we consider a 2-meter-high embankment intended to support asphalt, similar to the one in the Fig. 2 that was considered.

The embankment is constructed from low-deformability fine materials and is assumed to have an elastoplastic behavior. It will be subjected to hydro-mechanical stresses to evaluate the overall behavior of fine lateritic soils encountered in Sub-Saharan Africa for reuse in the construction of road infrastructure. The embankment is constructed in layers under unsaturated

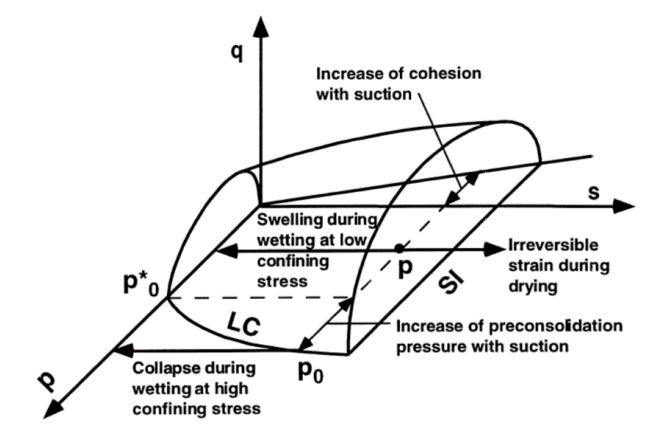


Fig. 1: 3D-view of yield surface in p - q - s stress space, (Ramon *et al.*, 2014)



Fig. 2: Embankment of the level crossing at the Kossodo roundabout (Ouagadougou)

Allows to known the state of stresses, the distribution of water content, porosity, and plastic parameters after construction stage.

Refinement for Simulation

In this paper, a purely numerical study of a road embankment is presented. The Barcelona thermoelastoplastic model has been used for this purpose. This model is derived from the Barcelona Base Model (BBM) and is designed to analyze the thermo-hydromechanical behavior of slightly deformable, water-unsaturated soils. This model is implemented in a numerical finite element code called CODE_BRIGHT (Olivella *et al.*, 2024). It is freely available and uses GiD graphical interface relatively easy-to-use. CODE_BRIGHT has been validated internationally by experimental studies

(Duan et al., 2024; Nguyen-Tuan, 2014; Ramon et al., 2014; Yubero et al., 2021).

Figure 3 shows the dike geometry. The construction process is described by Aviles et al., (2024). It is carried out in 0.25m layers under unsaturated conditions. Initial material, saturated at construction, is assumed to be 40%. To take account of local weather conditions, which induce significant water evaporation during construction, a water pressure of -20 MPa is set at the upper limit of the constructed layer. Finally, we assume that infiltration phenomena at the top of the structure and along the slope are negligible when construction finished. The base of the structure undergoes no horizontal or displacement. The geometry mesh comprises 1,287 quadratic tetrahedral elements with 1,392 nodes. To assess the long-term response of the structure to hydromechanical loads, the following boundary conditions were imposed:

- to take account of the effects of overloading by heavy vehicles on the structure, a load of 1 MPa (10 kg.cm⁻²) is applied to the upper surface. This value takes into account the maximum inflation pressure of 0.9 MPa for truck tires
- Burkina Faso is characterized by a long dry season and a relatively short winter season marked by heavy

rain (Gbohoui *et al.*, 2021). Abundant rainfall during the wet season causes the water table to rise, soaking earthen structures through capillary action. This phenomenon is taken into account by imposing a constant water flow of 2.314×10⁻⁴ kg.m⁻².s⁻¹ at the base of the structure

Table 1 summarizes the values of the parameters used. They are defined in CODE_BRIGHT user's guide (Olivella *et al.*, 2024). They were determined by Arnedo *et al.* (2005) on a silt-clay textured soil, similar to the one studied in our research project. Elasto-plastic parameters are obtained from oedometer and triaxial tests. Hydraulic parameters are derived from the water retention curve and a saturation permeability test.

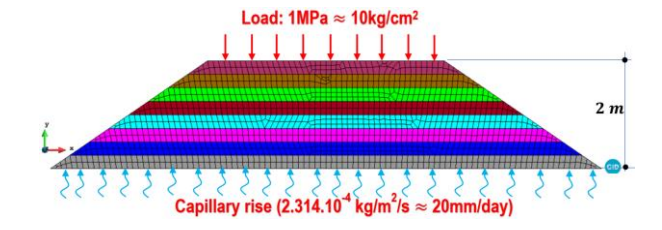


Fig. 3: Geometry, Mesh, and Boundary Conditions of the Embankment

Table 1: Values of parameters used for the simulation (Arnedo et al., 2005)

Elastic parameters $\kappa_{i0}(-)$	$\kappa_{s0}(-)$	$KMPa)_{min}$	v(-)	$\alpha_i(-)$	$p_{ref}(MPa)$
0.01	0	10	0.35	0	0.01
Plastic parameters					
$\lambda(0)$	r (-)	$\beta(MPa^{-1})$	$\rho(^{\circ}C^{-1})$	k (-)	$p_{s0}(MPa)$
0.075	0.75	35	0.1	0.01	0.1
$p_c(MPa)$	M (-)	α ₍₋₎	e ₀ (-)	$p_0^*(MPa)$	
0.1	1.1	0.99	0.59	0.1	
Hydrodynamic param	eters				
$P_0(MPa)$	$\sigma_0(N.m^{-1})$	$\lambda(-)$	$S_{rl}(-)$	$S_{ls}(-)$	$\phi_{ m o}$
1	0.072	0.5	0	1.0	0.35
$(k_{11})_0(m^2)$ 10^{-14}	$(k_{22})_0(m^2)$	$(k_{33})_0(m^2)$ 10^{-14}			
10^{-14}	10^{-14}	10^{-14}			

Results and Discussion

The following sections present the simulation results illustrating the stress and deformation evolution within the constructed road embankment.

Evolution of the Degree of Saturation

The saturation state of the embankment at the end of construction is shown in Fig. 4. It shows a low (less than 10%) and almost uniform saturation inside the structure, except at the edges, which are gradually drying. After construction, the structure is subjected to water stresses at the base due to capillary rise and mechanical loads at the top for 265 days, completing the construction phase in one

year. The saturation state of the structure in this case is presented in Fig. 5. A relatively significant increase in the embankment's saturation is observed compared to the end of the 90 days of construction. This increase is more pronounced at the slopes, gradually rising towards the upper edges. This variation is highlighted in Fig. 6, which represents saturation profiles at different positions of the embankment: from the base of the structure (h = 0 m) to its upper surface (h = 2 m). From the end of construction at 90 days, we observe an increase of more than 60% in the degree of saturation at the base after one year and about 30% at the surface. These results demonstrate the sensitivity of the material to capillary rise phenomena induced by the structures near the groundwater table. This

moistening process has more remarkable effects for soils with higher initial suction values (Sadeghabadi *et al.*, 2021). However, as shown in Fig. 1, the elastic domain extends more along suction (s) than along the other variables (p and q), so large variations in suction (s) are possible without hardening.

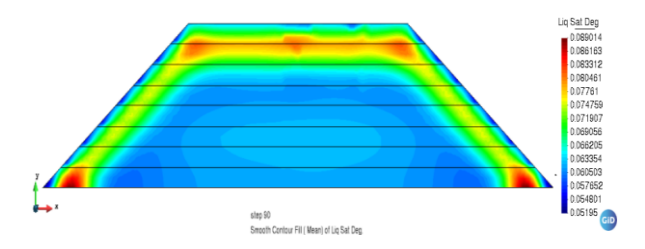


Fig. 4: Saturation state of the embankment at the end of construction (90 days mark)

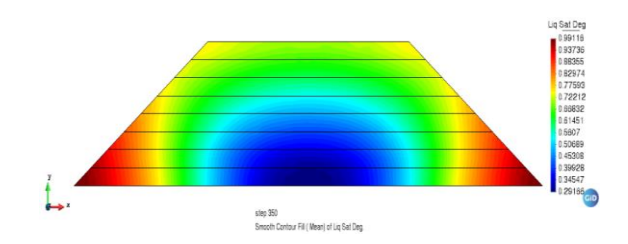


Fig. 5: Saturation state of the embankment 275 days after the end of construction (365 days mark)

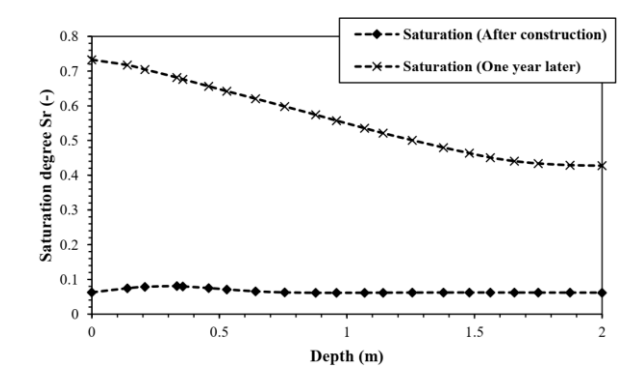


Fig. 6: Saturation degree profiles of the embankment at the end of construction (90 days) and 275 days post-construction (365 days)

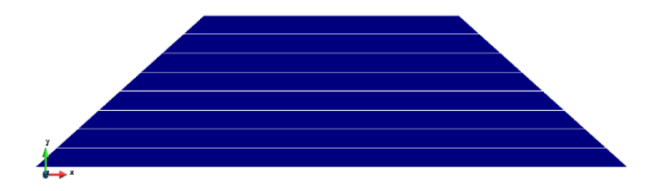


Fig. 7: Deformation state initialized to zero at the end of construction (90 days mark)

Deformations Experienced by the Embankment

During the construction phase, plastic deformations occur but are corrected by the addition of materials to achieve the desired configuration. To accurately assess the long-term deformations experienced by the structure, the post-construction state is considered intact with zero initial deformations. Fig. 7 illustrates this initial deformation state set to zero.

At the end of the construction phase, the structure was subjected to hydro-mechanical loading to evaluate the induced deformations, as shown in Fig. 8. Fig. 8(a) presents the recorded vertical deformations, which are more pronounced at the upper edges and in the middle of the embankment. These vertical deformations indicate settlement of the structure resulting from creep deformations. The horizontal deformations, shown in Fig. 8(b), reveal that the central part of the structure is less affected compared to the slopes, indicating lateral stretching of the embankment under the effect of mechanical loads. By overlaying the two types of deformations (Fig. 8(c)), we can identify the regions of the structure undergoing significant deformations and their orientations (Fig. 8(d)). Under these conditions, instability of the embankment slopes is observed when subjected to hydro-mechanical stresses at the base (water pressure) and at the upper surface (mechanical load).

Figure 9 illustrates the deformations along a vertical line at the center of the structure, from the base to the surface. A settlement of approximately 0.8 cm is recorded after 265 days of applied loading. These deformations confirm a collapse phenomenon in the road structure induced by wetting (Prajapati & Das, 2023), which could lead to surface layer degradation within a few years of service.

Evolution of Plastic Volumetric Deformation

The plasticity of fine soils, under the influence of their own weight and external loads, is characterized by a progressive transfer of these loads from the pore fluid pressure to the solid skeleton. This transfer occurs according to the spatial and temporal boundary conditions of the material, providing the soil with a certain level of resistance that makes it less deformable over time.

This state is illustrated in Fig. 10, which displays an increase in plastic volumetric deformation. This figure shows that plastic volumetric deformation intensifies over time and becomes more pronounced closer to the surface, which is primarily attributed to the effect of surface loads on soil plasticity. A plastic deformation of approximately 0.15% compared to the initial state (at the end of construction) is observed after 265 days of applied loads.

Study of Embankment Behavior Under Unsaturated Conditions Subjected to Hydraulic and Mechanical Loading

The evolution of the void ratio as a function of the applied vertical stress allows the evaluation of the material's compressibility through the compressibility curve presented in Fig. 11 for our case study. This curve helps determine the yield limit of the material, given by the pre-consolidation stress corresponding to the intersection of lines (D_1) and (D_2) , which is.

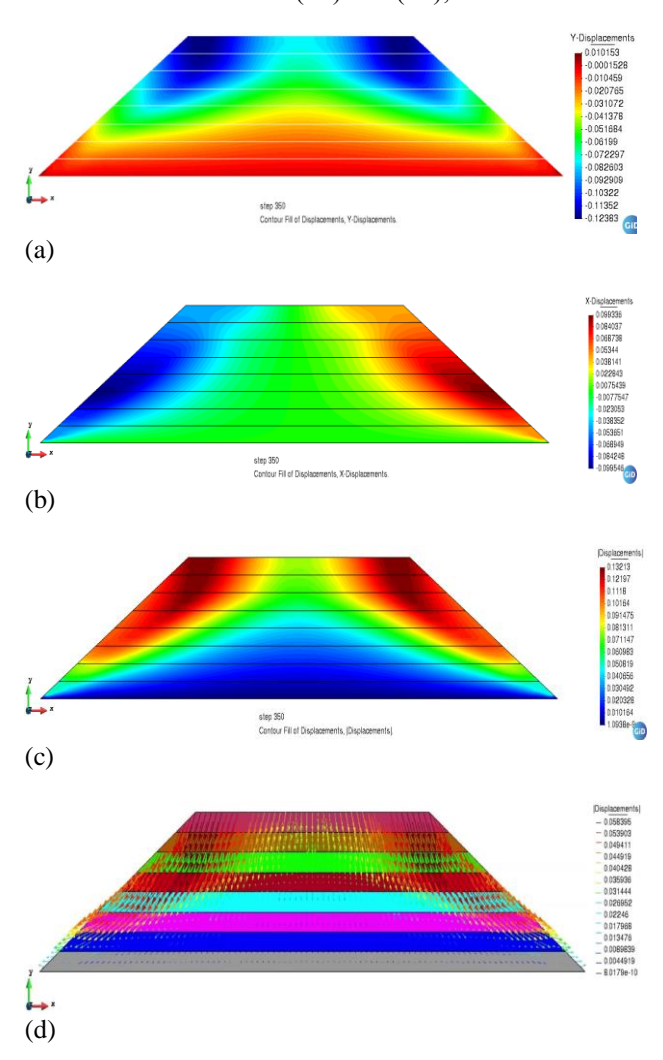


Fig. 8: Deformations experienced by the embankment 275 days after the end of construction (365 days mark): (a) Vertical deformations (b) Horizontal deformations (c) Combined vertical and horizontal deformations (d) Direction of deformations

 $p_0^* = 70$ kPa. Any mechanical load beyond this value will induce plastic deformations in the soil. Other compressibility characteristics, such as the compression index Cc and the swelling index Cs, can also be derived

from this curve. These are the slopes of lines (D_1) and (D_2) , respectively. For the material used in our embankment, the values of Cc and Cs are 0.12 and 0.009, respectively.

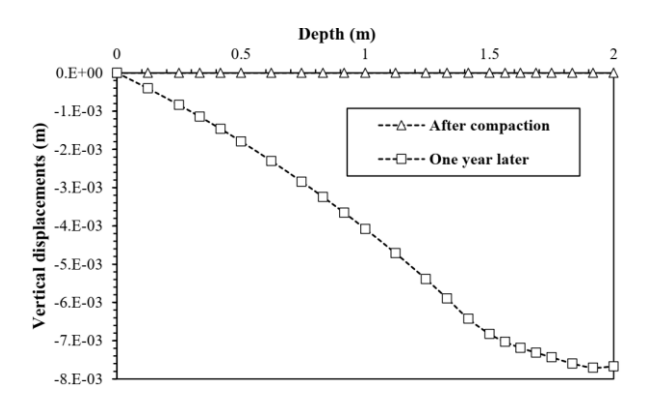


Fig. 9: Settlement profiles of the embankment recorded after 265 days of applied loading

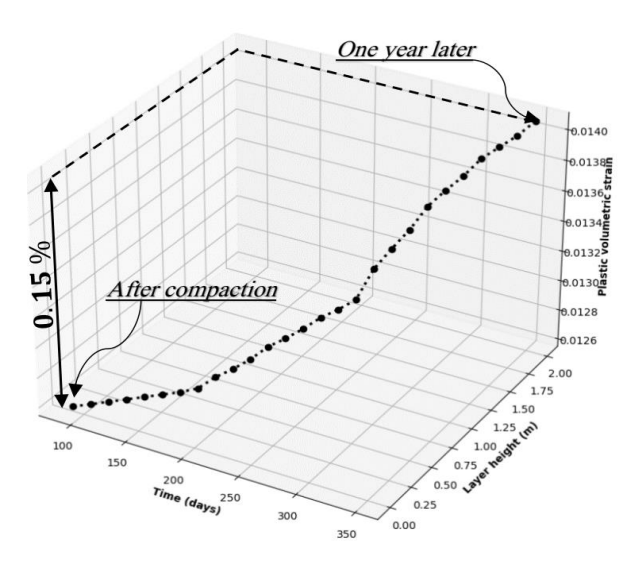


Fig. 10: Evolution of plastic volumetric deformation of the embankment

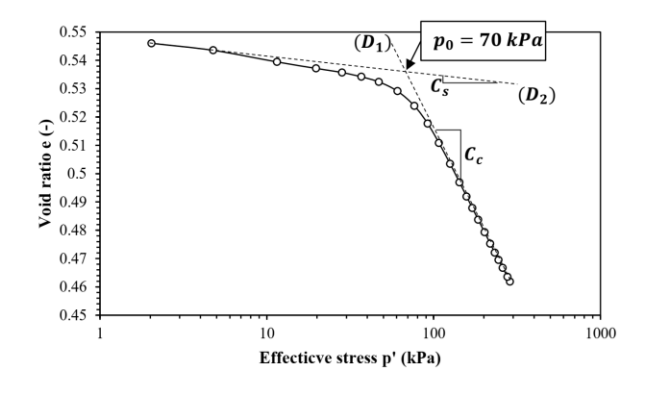


Fig. 11: Soil compressibility curve

We present in Fig. 12 the LC (Loading Collapse) curve, one of the boundary branches of the material's elasticity domain shown in Fig. 1. This curve illustrates the reduction in pre-consolidation pressure during soil wetting at the base. From this, we deduce a pre-consolidation pressure in the saturated state of the soil of $p_0^* = 2$ kPa. The analysis of this LC curve, which delineates the elastic and plastic deformation domains, reveals three behavior zones identified experimentally by Ouguemat *et al.* (2015); Gandema *et al.* (2020). Specifically, for all applied effective stresses p' such that $p' < p_0^*$, the behavior is solely elastic swelling during a reduction in suction.

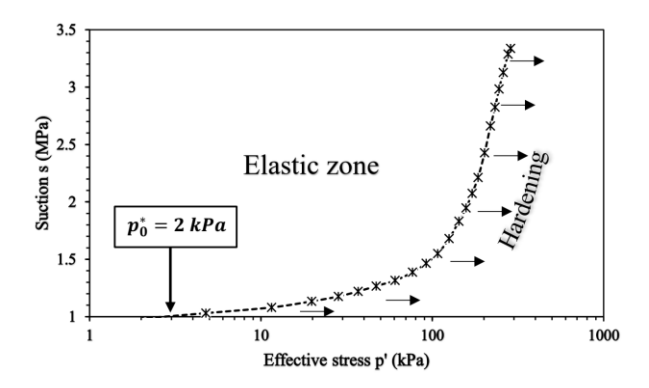


Fig. 12: LC Loading Surface

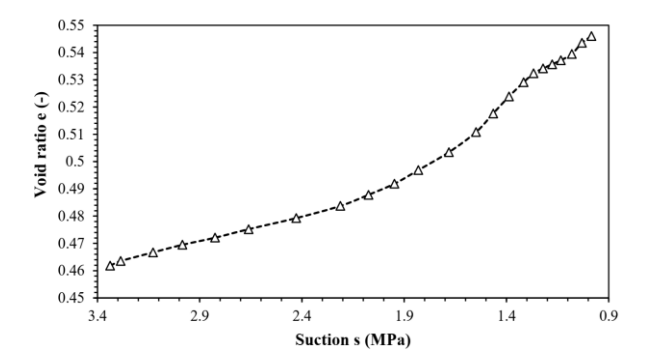


Fig. 13: Evolution of the void ratio during soil rewetting by capillary rise

An effective stress p', such that $p' > p_0^*$ and located within the elastic domain, will, during rewetting, first induce elastic swelling and then plastic collapse upon crossing the LC curve. Conversely, an effective stress outside the elastic domain results solely in plastic collapse during wetting. This plasticity alters (increases) the value of p_0^* , making it the current stress, thus shifting the entire LC curve and expanding the elastic domain, a phenomenon known as hardening, observed in Fig. 11.

The curve in Fig. 13 represents the volumetric response of the embankment as suction decreases due to

wetting caused by capillary rise. The observed increase in the void ratio implies softening of the material, reflected by a reduction in the compression index and preconsolidation pressure. This softening also affects shear strength through a reduction in cohesion. However, Khalilnejad *et al.* (2013) demonstrated that the friction angle remains independent of suction but appears to be related to soil properties such as density, water content, and plasticity index.

Conclusion

In this article, the long-term behavior of a 2-meter-high road embankment composed of compacted, unsaturated silty clay soil was analyzed using the Barcelona Basic Model for Thermo-Hydro-Mechanical Behavior of Expansive Clays (BBM-TEP) implemented in the finite element software CODE_BRIGHT. The study considered the effects of heavy vehicle loads and embankment wetting due to capillary rise. The main findings show that after 265 days of hydromechanical loading:

- There is a significant increase in saturation at the base of the embankment, from 10% at the end of construction to 72%. However, the considered capillary rise does not lead to full saturation of the embankment
- Deformations are particularly pronounced at the upper edges and slopes, indicating slope instability.
 A settlement of 0.8 cm was recorded at the center of the embankment
- Although the plasticity of the material was corrected by adding additional material during construction, a plastic volumetric deformation of 0.15% due to creep was observed
- The behavior of the embankment under unsaturated conditions was analyzed through the compressibility curve and LC loading surface, confirming the BBM-TEP model's capability to reliably reproduce the observed behaviors under environmental variables

Further studies could examine the impact of wettingdrying cycles, soil compositions, and initial compaction conditions on the long-term stability and hydromechanical response of embankments to optimize construction practices and reduce degradation risks.

Acknowledgment

The authors would like to express their sincere gratitude to the team of Professor Sebastia Olivella, Department of Civil and Environmental Engineering (DECA), Escola de Camins (ETSECCPB), Centre Internacional de Mètodes Numèrics en Enginyeria (CIMNE), Universitat Politècnica de Catalunya (UPC), Spain, for welcoming Mr. GANDEMA into their team

and for their continued support in using CODE BRIGHT. They would also like to pay tribute to the late Dr. François OUEDRAOGO, who was the linchpin of the team that introduced these themes in Burkina Faso. RIP.

Funding Information

This study is part of the implementation of the doctoral scholarship awarded to Mr. GANDEMA by the Higher Education Support Project (PAES) of Burkina Faso, financed by the World Bank.

Author's Contributions

Soumaïla Gandema: Study design, modeling, formal data analysis, data collection and investigation, methodological development, drafting of the initial manuscript, and critical revisions.

François Dabilgou: Contribution to study design, formal analysis, methodological development, review and revision of the manuscript.

Rimyalegdo Kiébré: Contribution to study conceptualization, data collection and investigation, methodological input, manuscript review and editing.

Timbe N'Djédanoum: Formal data analysis and drafting of sections of the initial manuscript.

Guillaume Zamantakonè Ki: Formal data analysis and drafting of sections of the initial manuscript.

Marcel Bawindsom Kébré: Study conceptualization, data collection and investigation, methodological development, critical review and editing of the manuscript.

Ethics

There are no ethical worries or concerns regarding this study.

References

- Ali, T., Showkat, R., & Babu, G. L. S. (2021). Hydro-Mechanical Simulations of Unsaturated Soil Slope. *Indian Geotechnical Journal*, *51*(4), 861–869. https://doi.org/10.1007/s40098-021-00554-3
- Alvar-Beltrán, J., Gobin, A., Orlandini, S., Dao, A., & Marta, A. (2021). Climate resilience of irrigated quinoa in semi-arid West Africa. *Climate Research*, 84, 97–111. https://doi.org/10.3354/cr01660
- Arnedo, D., Alonso, E., & Olivella, S. (2005). Canales en terraplén sobre suelo natural y compactado. *Ingeniería Civil*, 139, 68–80.
- Aviles, L. A., Di Carluccio, G., & Pinyol, N. M. (2024). Layered construction process with the material point method. *Computers and Geotechnics*, 171, 106401. https://doi.org/10.1016/j.compgeo.2024.106401

- Bakaiyang, L., Myriam, D. U. C., Boussafir, Y., Szymkiewicz, F., & Madjadoumbaye, J. (2022). Comportement des argiles gonflants de type Karal traitées pour une application routière.
- Cerema. (2023). Guide des Terrassements des remblais et des couches de forme, fascicule I, principes généraux.
- Chaiyaput, S., Arwaedo, N., Jamsawang, P., & Ayawanna, J. (2022). Natural Para Rubber in Road Embankment Stabilization. *Applied Sciences*, *12*(3), 1394. https://doi.org/10.3390/app12031394
- Droniuc, N. (2013). Étude par la méthode des éléments finis du comportement des remblais en sols fins compactés. *Proceedings of the 18th International Conference on Soil Mechanics and Geotechnical Engineering*, 1097–1100.
- Droniuc, N. (2013). Étude par la méthode des éléments finis du comportement des remblais en sols fins compactés. *Proceedings of the 18th International Conference on Soil Mechanics and Geotechnical Engineering*, 1097–1100.
- Duan, G., Song, F., Wang, H., Rodriguez-Dono, A., Wang, L., & Chen, J. (2024). Stability analysis of unsaturated loess slopes subjected to extreme rainfall incorporating creep effects. *Computers and Geotechnics*, 169, 106231. https://doi.org/10.1016/j.compgeo.2024.106231
- Gandema, S., Kébré, M. B., & Naon, B. (2020). Hydromechanical Behavior of Low-Swelling Soils Compacted at Low Water Content: Laboratory Study. *Engineering*, *12*(11), 824–838. https://doi.org/10.4236/eng.2020.1211058
- Gbohoui, Y. P., Paturel, J.-E., Tazen, F., Mounirou, L. A., Yonaba, R., Karambiri, H., & Yacouba, H. (2021). Impacts of climate and environmental changes on water resources: A multi-scale study based on Nakanbé nested watersheds in West African Sahel. *Journal of Hydrology: Regional Studies*, *35*, 100828. https://doi.org/10.1016/j.ejrh.2021.100828
- Gens, A., & Sánchez, M. (2010). Long-term Performance of Engineered Barrier Systems PEBS. DELIVEERABLE (DN: D3. 5-2), Formulation of a Model Suitable for Long Term Predictions, 1–24.
- Gens, A., & Sánchez, M. (2014). Long-term Performance of Engineered Barrier Systems PEBS.
- Ghosh, B., Fatahi, B., Khabbaz, H., Nguyen, H. H., & Kelly, R. (2021). Field study and numerical modelling for a road embankment built on soft soil improved with concrete injected columns and geosynthetics reinforced platform. *Geotestiles and Geomembranes*, 49(3), 804–824.
 - https://doi.org/10.1016/j.geotexmem.2020.12.010
- Grossegger, D., MacAskill, K., & Al-Tabbaa, A. (2024). A critical review of road network material stocks and flows: Current progress and what we can learn from it. *Resources, Conservation and Recycling*, 205, 107584.
 - https://doi.org/10.1016/j.resconrec.2024.107584

- Hudaykulov, R. M., & Aralov, D. E. (2024). Results of Laboratory Studies of Strengthening Subgrade Soil with Modifier. Structural Mechanics of Engineering Constructions and Buildings, 20(1), 84–93. https://doi.org/10.22363/1815-5235-2024-20-1-84-93
- Hudaykulov, R., Makhmudova, D., Ikramova, F., Rakhmonov, J., & Aralov, D. (2024). Mechanical properties of reinforced loess soils in road pavements. *E3S Web of Conferences*, *525*, 01006. https://doi.org/10.1051/e3sconf/202452501006
- Kayadelen, C., Altay, G., & Önal, Y. (2022). Numerical simulation and novel methodology on resilient modulus for traffic loading on road embankment. *International Journal of Pavement Engineering*, 23(9), 3212–3221.
 - https://doi.org/10.1080/10298436.2021.1886296
- Khalilnejad, A., Ali, F. Hj., Hashim, R., & Osman, N. (2013). Finite-Element Simulation for Contribution of Matric Suction and Friction Angle to Stress Distribution during Pulling-Out Process. *International Journal of Geomechanics*, 13(5), 527–532. https://doi.org/10.1061/(asce)gm.1943-5622.0000243
- Khemissa, M., & Mahamedi, A. (2014). Cement and lime mixture stabilization of an expansive overconsolidated clay. Applied Clay Science, 95, 104–110. https://doi.org/10.1016/j.clay.2014.03.017
- Kired, F., Šešlija, M., Milović, T., Starčev-Ćurčin, A., Bulatović, V., & Radović, N. (2023). Stabilization of Different Soil Types Using a Hydraulic Binder. *Buildings*, 13(8), 2040. https://doi.org/10.3390/buildings13082040
- Mestat, P. (2001). MOMIS: une base de données sur la modélisation numérique des remblais sur sols compressibles et sur la confrontation calculs-mesures in situ. *Bulletin-Laboratoires Des Ponts Et Chaussees*, 43–58.
- Morsy, A. M., Helm, P. R., El-Hamalawi, A., Smith, A., Hughes, P. N., Stirling, R. A., Dijkstra, T. A., Dixon, N., & Glendinning, S. (2023). Development of a Multiphase Numerical Modeling Approach for Hydromechanical Behavior of Clay Embankments Subject to Weather-Driven Deterioration. *Journal of Geotechnical and Geoenvironmental Engineering*, 149(8), 04023062.
 - https://doi.org/10.1061/jggefk.gteng-11213
- Mridakh, A. H., Ejjaaouani, H., Nguyen, B.-P., Lahlou, F., & Labied, H. (2022). Soft Soil Behavior Under High-Speed Railway Embankment Loading Using Numerical Modelling. *Geotechnical and Geological Engineering*, 40(5), 2751–2767. https://doi.org/10.1007/s10706-022-02059-z

- Nguyen-Tuan, L. (2014). Coupled thermo-hydromechanical analysis: Experiment and back analysis. *Dissertation, Bochum, Ruhr-Universit{\"a}t Bochum, I.* 1–108.
- Olivella, S., Rodriguez-Dono, A., & Vaunat, J. (2024). CODE BRIGHT 2024 User's Guide.
- Ouguemat, A., Jamin, F., & El Youssoufi, M. S. (2015). Compactage à faible teneur en eau de sols de remblais. *HAL Open Archive Communication in a Scientific Conference* (2015)., 1.
- Pallav, V., Teppand, T., Leinpuu, A., Shanskiy, M., Mets, M., Mändar, H., Rikmann, E., & Liiv, J. (2023). Stabilization of Road Embankments on Peat Soils Using Oil Shale Ash and Pozzolanic Additives. *Applied Sciences*, 13(14), 8366. https://doi.org/10.3390/app13148366
- Pereira, P. M., & Vieira, C. S. (2022). A Literature Review on the Use of Recycled Construction and Demolition Materials in Unbound Pavement Applications. *Sustainability*, 14(21), 13918. https://doi.org/10.3390/su142113918
- Rahla, K. M., Bragança, L., & Mateus, R. (2021). Practical strategies for embodying the circular economy concept in the construction sector. *In Sustainable Urban Development: Topics, Trends and Solutions*, 11–15. https://doi.org/10.1088/978-0-7503-3971-1ch15
- Ramon, V., Pinyol, N., Gens, A., & Alonso, E. (2014). *Long-term Performance of Engineered Barrier* Systems PEBS.
- Sadeghabadi, A., Noorzad, A., & Zad, A. (2022). An Extension to Barcelona Basic Model Predicting the Behavior of Unsaturated Soils. *Transportation Infrastructure Geotechnology*, 9(2), 133–154. https://doi.org/10.1007/s40515-021-00159-6
- Showkat, R., Mohammadi, H., & Babu, G. L. S. (2022). Effect of Rainfall Infiltration on the Stability of Compacted Embankments. *International Journal of Geomechanics*, 22(7).
 - https://doi.org/10.1061/(asce)gm.1943-5622.0002425
- Tulebekova, A., Zhussupbekov, A., Zhankina, A., Aldungarova, A., & Mamyrbekova, G. (2024). Practical experience in the construction of roads in difficult soil conditions. *Journal of Water and Land Development*, 60(1–3), 138–148. https://doi.org/10.24425/jwld.2024.149115
- Vukićević, M., Marjanović, M., Pujević, V., & Jocković, S. (2019). The Alternatives to Traditional Materials for Subsoil Stabilization and Embankments. *Materials*, 12(18), 3018. https://doi.org/10.3390/ma12183018
- Yubero, M. T., Olivella, S., Gens, A., Bonet, E., Lloret, A., & Alfonso, P. (2021). Analysis of the process of compaction movements of deposits of crushed salt tailings. *Engineering Geology*, 293, 106290. https://doi.org/10.1016/j.enggeo.2021.106290